

When, Where and to What Extent Do Temperature Perturbations near Tropical Deep Convection Follow Convective Quasi Equilibrium?

Yi-Xian Li¹, Hirohiko Masunaga², Hanii Takahashi³, and Jia-Yuh Yu¹

¹National Central University

²Nagoya University

³The Jet Propulsion Laboratory (JPL)

April 16, 2024

Abstract

Convective Quasi-Equilibrium (CQE) is often adopted as a useful closure assumption to summarize the effects of unresolved convection on large-scale thermodynamics, while existing efforts to observationally validate CQE largely rely on specific spatial domains or sites rather than the source of CQE constraints—deep convection. This study employs a Lagrangian framework to investigate leading temperature perturbation patterns near deep convection, of which the centers are located by use of an ensemble of satellite measurements. Temperature perturbations near deep convection with high peak precipitation are rapidly adjusted towards the CQE structure within the two hours centered on peak precipitation. The top 1% precipitating deep convection constrains the neighboring free-tropospheric leading perturbations up to 8 degrees. Notable CQE validity beyond a 1-degree radius is observed when peak precipitation exceeds the 95th percentile. These findings suggest that only a small fraction of deep convection with extreme precipitation shapes tropical free-tropospheric temperature patterns dominantly.

Hosted file

984155_0_art_file_11757980_s6z1d0.docx available at <https://authorea.com/users/714668/articles/698930-when-where-and-to-what-extent-do-temperature-perturbations-near-tropical-deep-convection-follow-convective-quasi-equilibrium>

1 **When, Where and to What Extent Do Temperature Perturbations near**
2 **Tropical Deep Convection Follow Convective Quasi Equilibrium?**

3 **Yi-Xian Li^{1,2,*}, Hirohiko Masunaga², Hanii Takahashi³ and Jia-Yuh Yu¹**

4 ¹Department of Atmospheric Sciences, National Central University, Taoyuan, Taiwan

5 ²Institute for Space-Earth Environmental Research, Nagoya University, Nagoya, Japan

6 ³Jet Propulsion Laboratory, California Institute of Technology, Pasadena, California, USA

7 **Key Points:**

- 8 • Tropical temperature perturbations near extreme deep convection rapidly conform to
9 convective quasi equilibrium in a two-hour window.
- 10 • Only the top 5% precipitating deep convection can modulate hourly tropical temperature
11 patterns beyond a 1-degree radius.
- 12 • Top 1% precipitating deep convection constrains nearby temperature perturbations up to
13 an 8-degree radius during peak precipitation.

14 *Correspondence author: Yi-Xian Li (Yi-Xian.Li@monash.edu)

15 **Abstract**

16 Convective Quasi-Equilibrium (CQE) is often adopted as a useful closure assumption to
17 summarize the effects of unresolved convection on large-scale thermodynamics, while existing
18 efforts to observationally validate CQE largely rely on specific spatial domains or sites rather
19 than the source of CQE constraints—deep convection. This study employs a Lagrangian
20 framework to investigate leading temperature perturbation patterns near deep convection, of
21 which the centers are located by use of an ensemble of satellite measurements. Temperature
22 perturbations near deep convection with high peak precipitation are rapidly adjusted towards the
23 CQE structure within the two hours centered on peak precipitation. The top 1% precipitating
24 deep convection constrains the neighboring free-tropospheric leading perturbations up to 8
25 degrees. Notable CQE validity beyond a 1-degree radius is observed when peak precipitation
26 exceeds the 95th percentile. These findings suggest that only a small fraction of deep convection
27 with extreme precipitation shapes tropical free-tropospheric temperature patterns dominantly.

28 **Plain language summary**

29 Convective Quasi-Equilibrium (CQE) is a concept in atmospheric science that explains a state
30 where the influence of deep convection (cumulonimbus clouds) and large-scale atmospheric
31 forces is balanced, causing certain thermodynamic properties close to specific reference profiles.
32 Previous studies have focused on how temperature changes relate to the CQE structure but in
33 specific regions or sites while this study aims areas near deep convection—supposedly the
34 source of CQE constraints. Using a unique framework with data from multiple satellites, we
35 tracked the evolution of temperature patterns near deep convection. We found that temperatures
36 near deep convection with extreme rainfall are adjusted towards the CQE structure rapidly within

37 2 hours of maximum rainfall. However, only the deep convection with top 5% extreme rainfall
38 can effectively affect nearby temperature pattern beyond 1 degree, with the top 1% influencing
39 up to an 8-degree radius. These findings highlight the dominant impact of a small fraction of
40 deep convection, particularly those with extreme rainfall, on nearby temperature patterns.

41 **1. Introduction**

42 The Convective Quasi-Equilibrium (CQE) theory, first introduced by Arakawa & Schubert
43 (1974) , posits that convective energy within cumulus ensemble remains in statistical
44 equilibrium, balanced between large-scale replenishment and cloud-scale consumption. Intrinsic
45 to the equilibrium, moist convection actively steers vertical temperature perturbations towards
46 specific reference profiles, a principle embedded in various moist convective adjustments
47 (Ahmed et al., 2020; Betts, 1973; Betts & Miller, 1986; Kuo, 1974; Manabe et al., 1965) and
48 parameterizations (Chikira & Sugiyama, 2010; Frierson, 2007; Moorthi & Suarez, 1992; Randall
49 & Pan, 1993; T. Wu, 2012; G. J. Zhang & McFarlane, 1995; Zhao et al., 2018). Such adjustment
50 of vertical temperature structures is facilitated by analytic solutions (Emanuel et al., 1994; Yu &
51 Neelin, 1997) to develop tropical intermediate complexity models (Neelin & Zeng, 2000; Sobel
52 & Neelin, 2006; Zeng et al., 2000) and has been found to be profound within deep convective
53 areas by observations (Holloway & Neelin, 2007; Li et al., 2022; W. Wu et al., 2006; Xu &
54 Emanuel, 1989).

55 Deep convection, often characterized by its robust updraft core and expansive cirrus anvil
56 canopy, has predominantly been studied using satellite observations to discern its
57 thermodynamic characteristics across temporal and spatial scales (Del Genio & Kovari, 2002;
58 Feng et al., 2011; Houze et al., 2015). Collocating polar-orbiting and geostationary satellites

59 enables the monitoring of three-dimensional thermodynamic structures within deep convection
60 (Chakraborty et al., 2016; Chung et al., 2008; Takahashi & Luo, 2014), among which is the
61 Mesoscale Convective System (MCS) playing a crucial role in contributing over half of tropical
62 precipitation (Feng et al., 2021; Nesbitt et al., 2006; Roca et al., 2014; Schumacher &
63 Rasmussen, 2020; Yuan & Houze, 2010). MCSs behave differently with and without diverse
64 deep convective cores (D. Wang et al., 2020; Zheng et al., 2018) while algorithms utilizing
65 geostationary satellites have been employed to track MCSs, generating comprehensive global
66 datasets (Feng et al., 2021; Fiolleau & Roca, 2013; Huang et al., 2018).

67 Despite extensive validations showing the proximity of tropical temperature perturbation profiles
68 to those constrained by the CQE theory, the spatial domains were confined to specific sites or
69 regions across observations (Holloway & Neelin, 2007; Li et al., 2022; Nie et al., 2010) and
70 models (Lin et al., 2015; X. Wang et al., 2022). This leaves an intriguing gap unexplored: the
71 immediate vicinity of tropical deep convection, presumed to be the primary force shaping
72 temperature structures. To bridge this gap, a Lagrangian framework integrating an MCS-tracking
73 database and CloudSat retrieval to pinpoint the center of deep convective systems is proposed to
74 quantitatively assess when the temperature perturbations, within a certain radius relative to the
75 center, adhere to the CQE structure.

76 **2. Data and Methodology**

77 **2.1. Data**

78 The CloudSat satellite is equipped with a 94 GHz Cloud Profiling Radar (CPR) that detects
79 cloud and precipitation particles. The CPR has a high-resolution footprint of approximately 1.7
80 km along track and 1.3 km across track with a vertical resolution of 480 m. Its active sensing

81 capabilities enable the radar data to provide detailed vertical cloud structures. The Tracking Of
82 Organized Convection Algorithm through a 3-D Segmentation (TOOCAN) is a specialized tool
83 developed for detecting and tracking MCS using infrared imagery from geostationary satellites
84 (Fioleau & Roca, 2013). The clustering method within TOOCAN utilizes an iterative process
85 across horizontal and temporal dimensions to decompose brightness temperature regions under
86 235 K into several MCSs by repeating growing regions starting at 190 K with a 5-K increment.
87 To identify deep convection, radar reflectivity and cloud mask data from the CloudSat satellite's
88 2B-GEOPROF product (Marchand et al., 2008), and morphological parameters of MCS mass
89 center locations (latitude, longitude, time) along the life cycles from the TOOCAN database, are
90 employed.

91 However, to obtain the most accurate representation of the atmosphere's true state, atmospheric
92 reanalysis combining observational data with numerical models, is commonly utilized. In this
93 study, we examine the hourly temperature field using the European Center for Medium-Range
94 Weather Forecasts' fifth global reanalysis (ERA-5), which is generated based on the Integrated
95 Forecasting System (IFS) Cy41r2 with a four-dimensional variational data assimilation scheme
96 (Hersbach et al., 2020). In addition to temperature data across all available pressure levels, we
97 also extract total precipitation data from the ERA5 to adjust the time coordinate for analysis.
98 Both TOOCAN and ERA-5 data are harmonized to a temporospatial resolution of $0.25^\circ \times 0.25^\circ$
99 and hourly increments to ensure their congruence.

100 Within the scope of this study, only MCS objects with track of the mass center confined within
101 30 degrees north and south in latitude over lands and oceans are examined. To align with the data
102 availability across the CloudSat, TOOCAN, and ERA-5, we analyze data only for the year 2013.

103 Note that only the ascending (daytime) observations of CloudSat at around local time 13:30 is
104 used here due to its battery anomaly since 2011.

105 **2.2. Locating centers of deep convection**

106 In this manuscript, we focus on well-developed MCSs that contain at least one deep convective
107 core (DCC), detected by CloudSat, within its coverage at any given time during its lifespan
108 recognized by TOOCAN. The DCC criteria encompass continuous radar echo from cloud top to
109 within 2 km of the surface, an echo of at least 10 dBZ above 10 km, and an attaching anvil
110 horizontally spanning over 20 km with its base above 5 km, similar to previous works
111 (Takahashi & Luo, 2012; Takahashi et al., 2017, 2021, 2023). This integration of continuous
112 monitoring from geostationary satellites and vertical-penetration ability from polar-orbiting
113 satellite prevents misclassification based solely on cold brightness temperature (Liu et al., 2007)
114 and facilitates accurate tracking of deep convection centers. Note that the TOOCAN data over
115 the western South Pacific is not available because the routine scanning schedule of the MTSAT-
116 2 satellite, being operated during the study period, did not allow as frequent observations as
117 optimal for cloud tracking in the southern hemisphere. Although the centers are ascertained using
118 integrating satellite products, subsequent Lagrangian analysis exclusively relies on ERA-5
119 reanalysis data due to its capacity to capture temporal evolution across a vast three-dimensional
120 domain equally inside and outside clouds unlike infrared satellite sounding.

121 **2.3. Characterizing temperature perturbations near deep convection**

122 All following calculations and illustrations in this section are conducted within a specified
123 radius, or the distance from the deep convection center chosen from 1 to 10 degrees, from the
124 convection centers. For each convection object, we identify the peak precipitation hour at every

125 grid throughout its life duration and extract the hourly temperature profiles within 24 hours
 126 before and after accordingly. The temperature perturbations are obtained by subtracting a mean
 127 temperature profile averaged over the relative [-24,24] hours within the radius. To investigate
 128 temperature behaviors influenced by convection intensity, a threshold for peak precipitation
 129 exceeding a specific percentile, ranging from 80% to 99%, is calculated and applied across the
 130 radial distance, relative hours, and convection objects. For each hour, the temperature
 131 perturbations conditioned on the peak precipitation over the 329 observed deep convective
 132 objects at each level are regressed against those in the free troposphere, defined between 850 and
 133 200 hPa, resulting in a single regression coefficient. The vertical profile of regression
 134 coefficients, same as that presented in Holloway & Neelin (2007), depicts the leading hourly
 135 pattern of temperature perturbations observed within the radius, reflective of a specific
 136 convection intensity.

137 **2.4. Quantifying similarity of temperature perturbations to the theoretical CQE structure**

138 The theoretical temperature perturbation profile constrained by CQE, to be compared with the
 139 leading observational profile, is referred to as the A-profile afterwards for simplicity. The A-
 140 profile is a function of temperature profile under assumptions of hydrostatic approximation, ideal
 141 gas law, and Clausius–Clapeyron relation (see detailed derivations in Li et al., 2022, modified
 142 from Yu & Neelin, 1997):

$$143 \quad A(p, T(p)) \equiv \frac{T'(p)}{T'(p_0)} = \left(\frac{p_{LCL}}{p_0}\right)^\kappa \frac{1+\gamma(T(p_{LCL}))}{1+\gamma(T(p))} \exp\left(-\kappa \int_p^{p_{LCL}} \frac{1}{1+\gamma(T(p'))} d\ln p'\right), p \leq p_{LCL}, \quad (1)$$

144 and

$$145 \quad A(p, T(p)) \equiv \left(\frac{p}{p_0}\right)^\kappa, p > p_{LCL}, \quad (2)$$

146 where p is pressure, T temperature, T' the temperature perturbation from climatology, p_0 the
147 reference level, p_{LCL} the lifting condensation level (LCL), $\gamma \equiv \frac{\varepsilon e_s l_v^2}{c_{pd} p R_v T^2}$ with $\varepsilon \equiv \frac{R_d}{R_v} = 0.622$ the
148 ratio of gas constant for dry air R_d to that for water vapor R_v , e_s the saturation vapor pressure
149 with respect to liquid, $l_v = 2.5 \times 10^6$ J/kg the latent heat of vaporization, $c_{pd} = 1004$ J/kg/K the
150 specific heat of dry air at constant pressure, and $\kappa \equiv \frac{R_d}{c_{pd}}$.

151 For simplicity, the individual A-profile is calculated with $p_0 = 1000$ hPa and $p_{LCL} = 950$ hPa by
152 input of temperature profile interpolated to a 5-hPa interval at each grid and hour, without
153 considering entrainment. To compare with the regression coefficient profiles, the A-profile is
154 averaged within the [-24, 24] hours and within the given radius, then normalized to have unity
155 root mean square over the free troposphere. Unless specifically noted, the term A-profile refers
156 to the normalized A-profile hereafter. These settings are considered practical given the robust
157 statistics of A-profiles in the tropics and the nature of A-profile illustrating proportions between
158 vertical levels (Li et al., 2022). Finally, to quantify similarity between the A-profile and
159 regression coefficient profile, vertical spatial correlation and root-mean-square deviation (RMSD)
160 are calculated over the free troposphere.

161 **3. Results and Discussions**

162 **3.1. Spatial distribution of temperature perturbations extracted near deep convection**

163 Prior to comparing the A-profile and regression coefficient profile for their similarity, we explore
164 the geographical distribution of collocated deep convection distribution to comprehend where the
165 temperature perturbations are analyzed.

166 Figure 1a shows the count of extracted temperature profiles spanning [-24, 24] hours near
167 tropical deep convection within a specific radius of 8 degrees from the deep convection centers,
168 irrespective of precipitation intensity. The 8-degree radius is selected because it represents the
169 maximum distance where the CQE constraint on temperature appears valid, as later detailed in
170 section 3.3. The pattern generally corresponds to the ITCZ climatology, with more deep
171 convection over the continents, especially the Amazon and west Africa, compared to the oceans.
172 To further examine the temperature structure in conjunction with extreme precipitation, Figure
173 1b manifests the number of extracted samples over grids where peak precipitation exceeds the
174 99th percentile of all instances. Similarly, it captures a greater prevalence of extreme convective
175 columns over continents than over oceans. The sensitivity tests with different radii demonstrate
176 no significant changes on the geographic patterns in both cases (not shown), where the land-sea
177 contrast of deep convection occurrences has been observed by previous studies (Liu & Zipser,
178 2005; Liu et al., 2007; Wang et al., 2019; Takahashi & Luo, 2014; Takahashi et al., 2017).

179 Note that Figure 1b does not mark where mass centers of deep convection or intense DCCs
180 locate but directly pinpoints the grids collocated with intense precipitation within the specified 8-
181 degree radius. Compared to an examination at the MCS scale, which analyzes every grid within
182 the radius of top 1%-precipitating MCSs (not shown), this analysis at the individual grid level
183 notably reduces noise among temperature perturbations. Such a difference likely arises due to
184 inhomogeneous precipitation pattern within MCSs and the spatial discrepancy between the
185 satellite-identified mass center and the ERA-5 precipitation center. The missing data over the
186 western South Pacific, roughly between 115°E-175°E, may appear concerning because of
187 frequent identification of DCCs (Takahashi & Luo, 2014; Takahashi et al., 2017). However, this
188 region contributes relatively less to the global occurrence of tropical deep convection observed

189 with coexisting high radar echo top height and low cloud-top brightness temperature (Liu et al.,
190 2007). Therefore, while the absence of data poses a constraint, its impact on the study's outcomes
191 and conclusions could be regarded as minor.

192 **3.2. Leading observations and their similarity to the CQE theoretical structure**

193 To derive the representative profile of observational temperature perturbations for comparison
194 with the A-profile, or the CQE theoretical structure, we adopt the regression method from
195 Holloway & Neelin (2007). Figures 2a-2g display the A-profile (dashed line) and leading
196 observational patterns (colored lines) obtained through the regression at specific hours relative to
197 the peak precipitation with a 7-hour interval, and Figure 2h collects all these profiles for a
198 comprehensive comparison. Note that the profiles are calculated using temperature profiles
199 conditioned on the 99th percentile peak precipitation (8.337 mm/hr) within an 8-degree radius of
200 the deep convection centers, corresponding to the 10555 occurrences distributed in Figure 1b. To
201 quantify the similarity between the regression coefficient profile and A-profile, Figure 2i
202 showcases the time series of RMSD and vertical spatial correlation, both computed over the free
203 troposphere between 850 and 200 hPa at each hour. Of special note is that the vertical spatial
204 correlation is identical to the cosine similarity between profiles, and hence a positive correlation
205 suggests a leading temperature perturbation profile that increases with height, mirroring the A-
206 profile pattern within the free troposphere. All correlations mentioned in the text refer to the
207 vertical spatial correlation.

208 Throughout most hours, the leading temperature perturbations tend to decrease with altitude in
209 the free troposphere, opposing that seen in the A-profile, as depicted in Figures 2a-2c and 2e-2g.
210 This leads to negative correlations and elevated RMSD in Figure 2i, suggesting that at an hourly

211 scale or within a day, the CQE principle is mostly limited (Donner & Phillips, 2003; Zhang,
212 2003; Lin et al., 2015). In contrast, the highest correlation and lowest RMSD occur at the peak
213 hour, flanked by abrupt increases within the [-4, 2] hour range. This is consistent with Figure 2d,
214 which captures similar increasing perturbations with height between both profiles over the free
215 troposphere, remarkably closely aligned between 700 and 300 hPa. The convective cold top,
216 marked by a negative minimal perturbation around 100 hPa (Holloway & Neelin, 2007), remains
217 consistently robust across all the hours. All the observational characteristics mentioned above
218 hold true when assessed across different radii and peak-precipitation thresholds within the [90th,
219 99th] percentile range except for the higher correlations found for tighter radii and stricter
220 thresholds (not shown). The rest of the manuscript will exclusively utilize the correlation to
221 assess the CQE validity on temperature, as RMSD exhibits a similar response with opposite
222 trend.

223 **3.3. CQE validity as a function of relative hour, relative distance and peak precipitation** 224 **percentile**

225 We have demonstrated how top-1%-precipitating temperature perturbations align with the A-
226 profile near deep convection, focusing on evolution of the vertical leading patterns. To provide a
227 more comprehensive scrutiny, we validate the proximity of temperature perturbations to the CQE
228 structure using spatial vertical correlation as a function of the hour relative to peak precipitation,
229 distance relative to the deep convection centers, and the threshold percentile of the peak
230 precipitation.

231 Figure 3a suggests that the CQE robustly constrains the leading temperature perturbations within
232 the [-1, 1] hour. The positive correlation reaches the farthest distance of 8 degrees during the

233 peak hour, along with the maximum correlation of ~ 0.87 among all hours. The robustness of the
234 CQE constraints on temperature within the 2 hours aligns with the timescale of convective
235 adjustment commonly considered (see section 5b in a review of Arakawa, 2004). This supports
236 the CQE principle that convective adjustment is relatively fast compared to large-scale forcing.
237 Interestingly, the influence of the CQE on temperature appears more profound one hour before
238 the peak precipitation, where the positive correlation reaches 7 degrees, compared to one hour
239 after, where it reaches 3 degrees. Such asymmetric horizontal extent of validity can be observed
240 by conditioning on percentiles higher than 96% (not shown). The CQE constraints on
241 temperature quickly deteriorate after one hour following the peak precipitation, causing
242 temperature perturbations to deviate from the CQE more rapidly than the build-up of positive
243 correlations before the peak hour. This aligns with the observations that the peak of the first
244 baroclinic mode, or deep convective mode favoring the CQE structure, is followed by the peak
245 of second baroclinic mode, which on the contrary disfavors the CQE (Masunaga & L'Ecuyer,
246 2014).

247 Notably, other positive correlations appear around $[-17, -15]$ and $[12, 14]$ hours, primarily
248 confined within a 1-degree radius. The hourly time series of maximum precipitation among the
249 top 1% precipitating grids suggests that this phenomenon is likely due to a few extreme
250 precipitation events which happen to peak around these hours (not shown) while these minor
251 peak correlations are more pronounced when considering a smaller radius and higher peak
252 precipitation (not shown).

253 Figure 3b demonstrates that during the hour of peak precipitation, only the leading temperature
254 perturbations with the top 10% peak precipitation exhibit a comparable pattern of increasing

255 perturbations with height, akin to the CQE structure within a 1-degree radius, while only those in
256 the top 5% extend beyond 1 degree. This suggests that not all convective objects can effectively
257 adjust the neighboring temperature through the CQE constraints, but only the extreme ones
258 among deep convection. This is consistent with the "circus tent" concept, which suggests that
259 deep convection with the highest free-tropospheric moist static energy or temperature play a
260 dominant role in convective adjustment processes in the tropics (Williams et al., 2023). The high
261 threshold of peak precipitations and the minor peaks of positive correlations in Figure 3 both
262 reinforce our understanding that most of the CQE constraints arise from a very small fraction of
263 deep convection.

264 **4. Concluding Remarks**

265 Although previous studies have extensively examined the validity of CQE on temperature, many
266 of them have focused on specific spatial domains or sites, rather than directly addressing the
267 source of CQE constraints—deep convection. This study aims to investigate the evolution of
268 leading temperature perturbation patterns near deep convection, consisting of MCSs identified by
269 stationary satellites and deep convective cores observed by the CloudSat at a time. By employing
270 a Lagrangian framework following the deep convection centers, this approach enables the
271 quantification of when, where, and to what extent these perturbations resemble the CQE
272 structure. Our key findings can be succinctly summarized as follows:

- 273 • (When) Conditioned on the top 1% peak precipitation and within the relative [-1, 1]
274 hours,

- 275 • (Where) temperature perturbations obeying the CQE structure, defined as a positive
276 vertical spatial correlation between the free-tropospheric leading observational and
277 analytic theoretical profiles, reaches a distance up to 8 degrees,
- 278 • (To what extent) accompanied by higher correlations before the peak precipitation than
279 after, with a maximum correlation of ~ 0.87 during the peak hour.

280 These results suggest that temperature perturbations near deep convection are rapidly
281 adjusted towards the CQE structure in a few hours, consistent with the idea that the weak
282 temperature gradient approximation allows tropical gravity waves to rapidly propagate strong
283 signals from deep convection to affect the surrounding environmental temperature (Ahmed et
284 al., 2021; Sobel et al., 2001; Y. Zhang & Fueglistaler, 2020). Within such a short timeframe,
285 on the order of an hour, the CQE's influence on temperature is noticeable only when
286 analyzing grids where peak precipitation exceeds the 90th percentile, implying that only a
287 small fraction of deep convection is capable of influencing the neighboring temperature over
288 distances greater than 100 kilometers. Temperature perturbations with the top 1% peak
289 precipitation near deep convection conform to the CQE structure up to 8 degrees from the
290 centers during the peak hour, as one might expect from the typical Rossby radius of
291 deformation, which ranges from hundreds to thousands of kilometers. Most importantly, this
292 study underscores the dominant role of deep convection with extreme precipitation in
293 shaping the leading patterns of tropical free-tropospheric temperature. One might consider
294 the possibility that the CQE theory has been considered valid at a timescale longer than a day
295 because the occurrence of extreme deep convection, which is capable of adjusting large-scale
296 temperature over a long distance, is not frequent within a day.

297 The current study provides an interesting angle in understanding how valid the CQE
298 constrains tropical free-tropospheric temperature near the deep convection in a Lagrangian
299 view. However, owing to the requirement of monitoring vertical temperature structure
300 changes with a high spatiotemporal resolution, the ERA-5 reanalysis data is utilized here
301 instead of comparable satellite observations as those used during the collocation of deep
302 convection. Also, although the collocation strengthens our confidence of collecting well-
303 developed MCSs coincided with deep convective cores at a certain time point, one cannot
304 assure that deep clouds always exist around the mass centers along the evolution. Overall, we
305 consider the methodological framework to be highly optimized for such an analysis but
306 future work improving the collocating procedures and expanding the studying period, even
307 towards how the CQE validity might change under a climate-change scale, is needed to
308 further understand the relationship between the CQE and deep convection.

309 **Acknowledgments**

310 YXL was supported by the National Science and Technology Council in Taiwan through Grants
311 111-2811-M-008-062 and 112-2917-I-564-008.

312 We express our gratitude to Dr. Thomas Fiolleau for his valuable discussions regarding the
313 TOOCAN database and for granting public access to it.

314 **Data Availability Statement**

315 Information about the CloudSat can be accessed through the CloudSat Data Processing Center
316 hosted at: <https://www.cloudsat.cira.colostate.edu/> while the level-2 radar data used here is
317 available at: <https://www.cloudsat.cira.colostate.edu/data-products/2b-geoprof>. Details regarding

318 the Tracking Of Organized Convection Algorithm using a 3-dimensional segmentation
319 (TOOCAN) can be found at <https://toocan.ipsl.fr/> while the database descriptions are available
320 at <https://doi.org/10.14768/20191112001.1>. The hourly temperature and precipitation data from
321 ERA-5 are obtained from <https://doi.org/10.24381/cds.bd0915c6> and
322 <https://doi.org/10.24381/cds.adbb2d47>, respectively.

References

- 324 Ahmed, F., Adames, Á. F., & Neelin, J. D. (2020). Deep Convective Adjustment of Temperature and Moisture.
325 *Journal of the Atmospheric Sciences*, **77**(6), 2163-2186. <https://doi.org/10.1175/JAS-D-19-0227.1>
- 326 Ahmed, F., Neelin, J. D., & Adames, Á. F. (2021). Quasi-Equilibrium and Weak Temperature Gradient Balances in
327 an Equatorial Beta-Plane Model. *Journal of the Atmospheric Sciences*, **78**(1), 209-227.
328 <https://doi.org/10.1175/JAS-D-20-0184.1>
- 329 Arakawa, A., & Schubert, W. H. (1974). Interaction of a Cumulus Cloud Ensemble with the Large-Scale
330 Environment, Part I. *Journal of the Atmospheric Sciences*, **31**(3), 674-701. [https://doi.org/10.1175/1520-0469\(1974\)031<0674:IOACCE>2.0.CO;2](https://doi.org/10.1175/1520-0469(1974)031<0674:IOACCE>2.0.CO;2)
- 331
- 332 Betts, A. K. (1973). Non-precipitating cumulus convection and its parameterization. *Quarterly Journal of the Royal
333 Meteorological Society*, **99**(419), 178-196. <https://doi.org/10.1002/qj.49709941915>
- 334 Betts, A. K., & Miller, M. J. (1986). A new convective adjustment scheme. Part II: Single column tests using GATE
335 wave, BOMEX, ATEX and arctic air-mass data sets. *Quarterly Journal of the Royal Meteorological
336 Society*, **112**(473), 693-709. <https://doi.org/10.1002/qj.49711247308>
- 337 Chakraborty, S., Fu, R., Massie, S. T., & Stephens, G. (2016). Relative influence of meteorological conditions and
338 aerosols on the lifetime of mesoscale convective systems. *Proceedings of the National Academy of
339 Sciences*, **113**(27), 7426-7431. <https://doi.org/10.1073/pnas.1601935113>
- 340 Chikira, M., & Sugiyama, M. (2010). A Cumulus Parameterization with State-Dependent Entrainment Rate. Part I:
341 Description and Sensitivity to Temperature and Humidity Profiles. *Journal of the Atmospheric Sciences*,
342 **67**(7), 2171-2193. <https://doi.org/10.1175/2010JAS3316.1>
- 343 Chung, E.-S., Sohn, B.-J., & Schmetz, J. (2008). CloudSat shedding new light on high-reaching tropical deep
344 convection observed with Meteosat. *Geophysical Research Letters*, **35**(2).
345 <https://doi.org/10.1029/2007GL032516>
- 346 Del Genio, A. D., & Kovari, W. (2002). Climatic Properties of Tropical Precipitating Convection under Varying
347 Environmental Conditions. *Journal of Climate*, **15**(18), 2597-2615. [https://doi.org/10.1175/1520-0442\(2002\)015<2597:CPOTPC>2.0.CO;2](https://doi.org/10.1175/1520-0442(2002)015<2597:CPOTPC>2.0.CO;2)
- 348
- 349 Emanuel, K. A., David Neelin, J., & Bretherton, C. S. (1994). On large-scale circulations in convecting
350 atmospheres. *Quarterly Journal of the Royal Meteorological Society*, **120**(519), 1111-1143.
351 <https://doi.org/10.1002/qj.49712051902>
- 352 Feng, Z., Dong, X., Xi, B., Schumacher, C., Minnis, P., & Khaiyer, M. (2011). Top-of-atmosphere radiation budget
353 of convective core/stratiform rain and anvil clouds from deep convective systems. *Journal of Geophysical
354 Research: Atmospheres*, **116**(D23). <https://doi.org/10.1029/2011JD016451>
- 355 Feng, Z., Leung, L. R., Liu, N., Wang, J., Houze Jr, R. A., Li, J., et al. (2021). A Global High-Resolution Mesoscale
356 Convective System Database Using Satellite-Derived Cloud Tops, Surface Precipitation, and Tracking.
357 *Journal of Geophysical Research: Atmospheres*, **126**(8), e2020JD034202.
358 <https://doi.org/10.1029/2020JD034202>
- 359 Fiolleau, T., & Roca, R. (2013). An Algorithm for the Detection and Tracking of Tropical Mesoscale Convective
360 Systems Using Infrared Images From Geostationary Satellite. *IEEE Transactions on Geoscience and
361 Remote Sensing*, **51**(7), 4302-4315. <https://doi.org/10.1109/TGRS.2012.2227762>
- 362 Frierson, D. M. W. (2007). The Dynamics of Idealized Convection Schemes and Their Effect on the Zonally
363 Averaged Tropical Circulation. *Journal of the Atmospheric Sciences*, **64**(6), 1959-1976.
364 <https://doi.org/10.1175/JAS3935.1>
- 365 Hersbach, H., Bell, B., Berrisford, P., Hirahara, S., Horányi, A., Muñoz-Sabater, J., et al. (2020). The ERA5 global
366 reanalysis. *Quarterly Journal of the Royal Meteorological Society*, **146**(730), 1999-2049.
367 <https://doi.org/10.1002/qj.3803>
- 368 Holloway, C. E., & Neelin, J. D. (2007). The Convective Cold Top and Quasi Equilibrium. *Journal of the
369 Atmospheric Sciences*, **64**(5), 1467-1487. <https://doi.org/10.1175/JAS3907.1>
- 370 Houze, R. A. J., Rasmussen, K. L., Zuluaga, M. D., & Brodzik, S. R. (2015). The variable nature of convection in
371 the tropics and subtropics: A legacy of 16 years of the Tropical Rainfall Measuring Mission satellite.
372 *Reviews of Geophysics*, **53**(3), 994-1021. <https://doi.org/10.1002/2015RG000488>
- 373 Huang, X., Hu, C., Huang, X., Chu, Y., Tseng, Y.-h., Zhang, G. J., & Lin, Y. (2018). A long-term tropical
374 mesoscale convective systems dataset based on a novel objective automatic tracking algorithm. *Climate
375 Dynamics*, **51**(7), 3145-3159. <https://doi.org/10.1007/s00382-018-4071-0>

376 Kuo, H. L. (1974). Further Studies of the Parameterization of the Influence of Cumulus Convection on Large-Scale
377 Flow. *Journal of the Atmospheric Sciences*, **31**(5), 1232-1240. <https://doi.org/10.1175/1520->
378 [0469\(1974\)031<1232:FSOTPO>2.0.CO;2](https://doi.org/10.1175/1520-0469(1974)031<1232:FSOTPO>2.0.CO;2)

379 Li, Y.-X., Neelin, J. D., Kuo, Y.-H., Hsu, H.-H., & Yu, J.-Y. (2022). How Close Are Leading Tropical Tropospheric
380 Temperature Perturbations to Those under Convective Quasi Equilibrium? *Journal of the Atmospheric*
381 *Sciences*, **79**(9), 2307-2321. <https://doi.org/10.1175/JAS-D-21-0315.1>

382 Lin, J.-L., Qian, T., Shinoda, T., & Li, S. (2015). Is the Tropical Atmosphere in Convective Quasi-Equilibrium?
383 *Journal of Climate*, **28**(11), 4357-4372. <https://doi.org/10.1175/JCLI-D-14-00681.1>

384 Liu, C., Zipser, E. J., & Nesbitt, S. W. (2007). Global Distribution of Tropical Deep Convection: Different
385 Perspectives from TRMM Infrared and Radar Data. *Journal of Climate*, **20**(3), 489-503.
386 <https://doi.org/10.1175/JCLI4023.1>

387 Manabe, S., Smagorinsky, J., & Strickler, R. F. (1965). SIMULATED CLIMATOLOGY OF A GENERAL
388 CIRCULATION MODEL WITH A HYDROLOGIC CYCLE. *Monthly Weather Review*, **93**(12), 769-798.
389 [https://doi.org/10.1175/1520-0493\(1965\)093<0769:SCOAGC>2.3.CO;2](https://doi.org/10.1175/1520-0493(1965)093<0769:SCOAGC>2.3.CO;2)

390 Marchand, R., Mace, G. G., Ackerman, T., & Stephens, G. (2008). Hydrometeor Detection Using Cloudsat—An
391 Earth-Orbiting 94-GHz Cloud Radar. *Journal of Atmospheric and Oceanic Technology*, **25**(4), 519-533.
392 <https://doi.org/10.1175/2007JTECHA1006.1>

393 Masunaga, H., & L'Ecuyer, T. S. (2014). A Mechanism of Tropical Convection Inferred from Observed Variability
394 in the Moist Static Energy Budget. *Journal of the Atmospheric Sciences*, **71**(10), 3747-3766.
395 <https://doi.org/10.1175/JAS-D-14-0015.1>

396 Moorthi, S., & Suarez, M. J. (1992). Relaxed Arakawa-Schubert. A Parameterization of Moist Convection for
397 General Circulation Models. *Monthly Weather Review*, **120**(6), 978-1002. <https://doi.org/10.1175/1520->
398 [0493\(1992\)120<0978:RASAP0>2.0.CO;2](https://doi.org/10.1175/1520-0493(1992)120<0978:RASAP0>2.0.CO;2)

399 Neelin, J. D., & Zeng, N. (2000). A Quasi-Equilibrium Tropical Circulation Model—Formulation. *Journal of the*
400 *Atmospheric Sciences*, **57**(11), 1741-1766. <https://doi.org/10.1175/1520->
401 [0469\(2000\)057<1741:AQETCM>2.0.CO;2](https://doi.org/10.1175/1520-0469(2000)057<1741:AQETCM>2.0.CO;2)

402 Nesbitt, S. W., Cifelli, R., & Rutledge, S. A. (2006). Storm Morphology and Rainfall Characteristics of TRMM
403 Precipitation Features. *Monthly Weather Review*, **134**(10), 2702-2721. <https://doi.org/10.1175/MWR3200.1>

404 Nie, J., Boos, W. R., & Kuang, Z. (2010). Observational Evaluation of a Convective Quasi-Equilibrium View of
405 Monsoons. *Journal of Climate*, **23**(16), 4416-4428. <https://doi.org/10.1175/2010JCLI3505.1>

406 Randall, D. A., & Pan, D.-M. (1993). Implementation of the Arakawa-Schubert Cumulus Parameterization with a
407 Prognostic Closure. In K. A. Emanuel & D. J. Raymond (Eds.), *The Representation of Cumulus Convection*
408 *in Numerical Models* (pp. 137-144). Boston, MA: American Meteorological Society.
409 https://doi.org/10.1007/978-1-935704-13-3_11

410 Roca, R., Aublanc, J., Chambon, P., Fiolleau, T., & Viltard, N. (2014). Robust Observational Quantification of the
411 Contribution of Mesoscale Convective Systems to Rainfall in the Tropics. *Journal of Climate*, **27**(13),
412 4952-4958. <https://doi.org/10.1175/JCLI-D-13-00628.1>

413 Schumacher, R. S., & Rasmussen, K. L. (2020). The formation, character and changing nature of mesoscale
414 convective systems. *Nature Reviews Earth & Environment*, **1**(6), 300-314. <https://doi.org/10.1038/s43017->
415 [020-0057-7](https://doi.org/10.1038/s43017-020-0057-7)

416 Sobel, A. H., & Neelin, J. D. (2006). The boundary layer contribution to intertropical convergence zones in the
417 quasi-equilibrium tropical circulation model framework. *Theoretical and Computational Fluid Dynamics*,
418 **20**(5), 323-350. <https://doi.org/10.1007/s00162-006-0033-y>

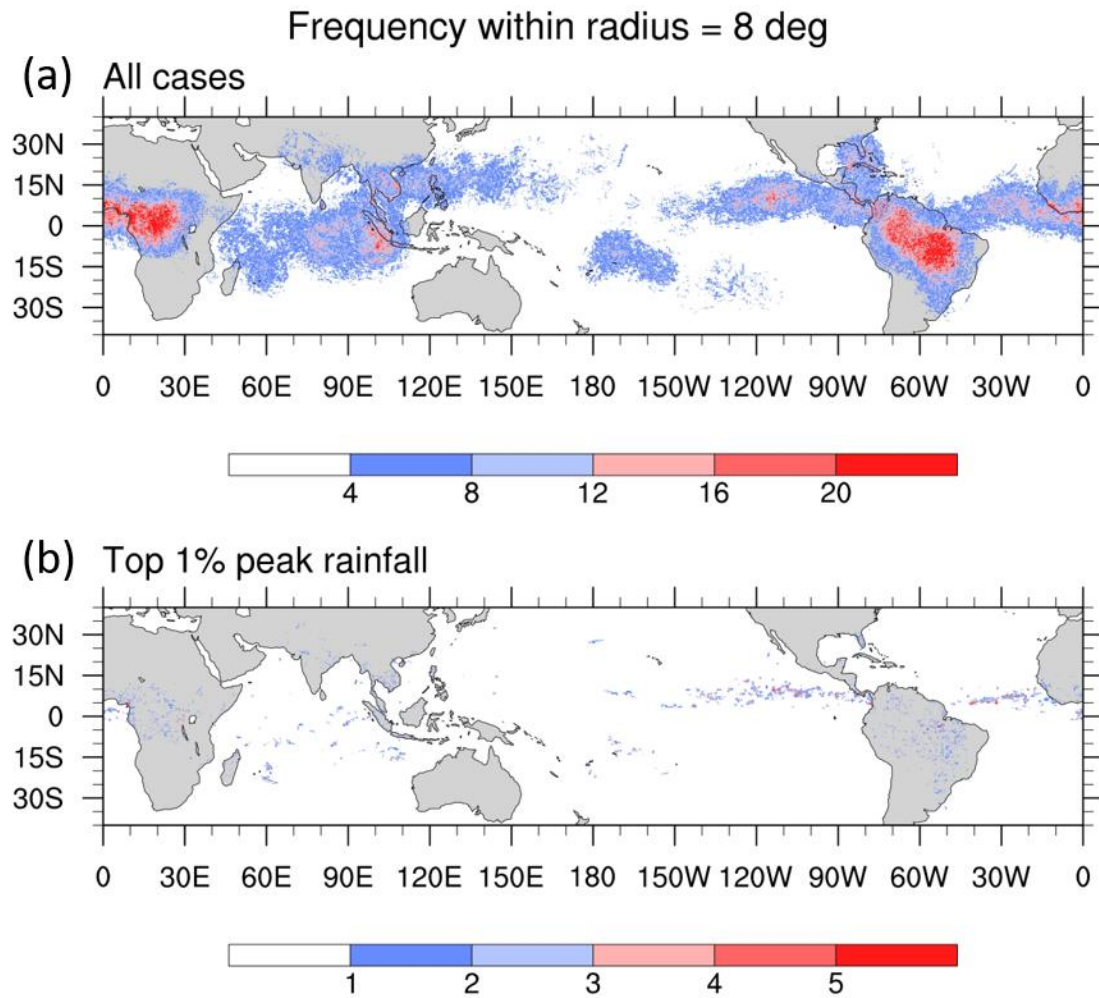
419 Sobel, A. H., Nilsson, J., & Polvani, L. M. (2001). The Weak Temperature Gradient Approximation and Balanced
420 Tropical Moisture Waves. *Journal of the Atmospheric Sciences*, **58**(23), 3650-3665.
421 [https://doi.org/10.1175/1520-0469\(2001\)058<3650:TWTGAA>2.0.CO;2](https://doi.org/10.1175/1520-0469(2001)058<3650:TWTGAA>2.0.CO;2)

422 Takahashi, H., & Luo, Z. (2012). Where is the level of neutral buoyancy for deep convection? *Geophysical*
423 *Research Letters*, **39**(15). <https://doi.org/10.1029/2012GL052638>

424 Takahashi, H., & Luo, Z. J. (2014). Characterizing tropical overshooting deep convection from joint analysis of
425 CloudSat and geostationary satellite observations. *Journal of Geophysical Research: Atmospheres*, **119**(1),
426 112-121. <https://doi.org/10.1002/2013JD020972>

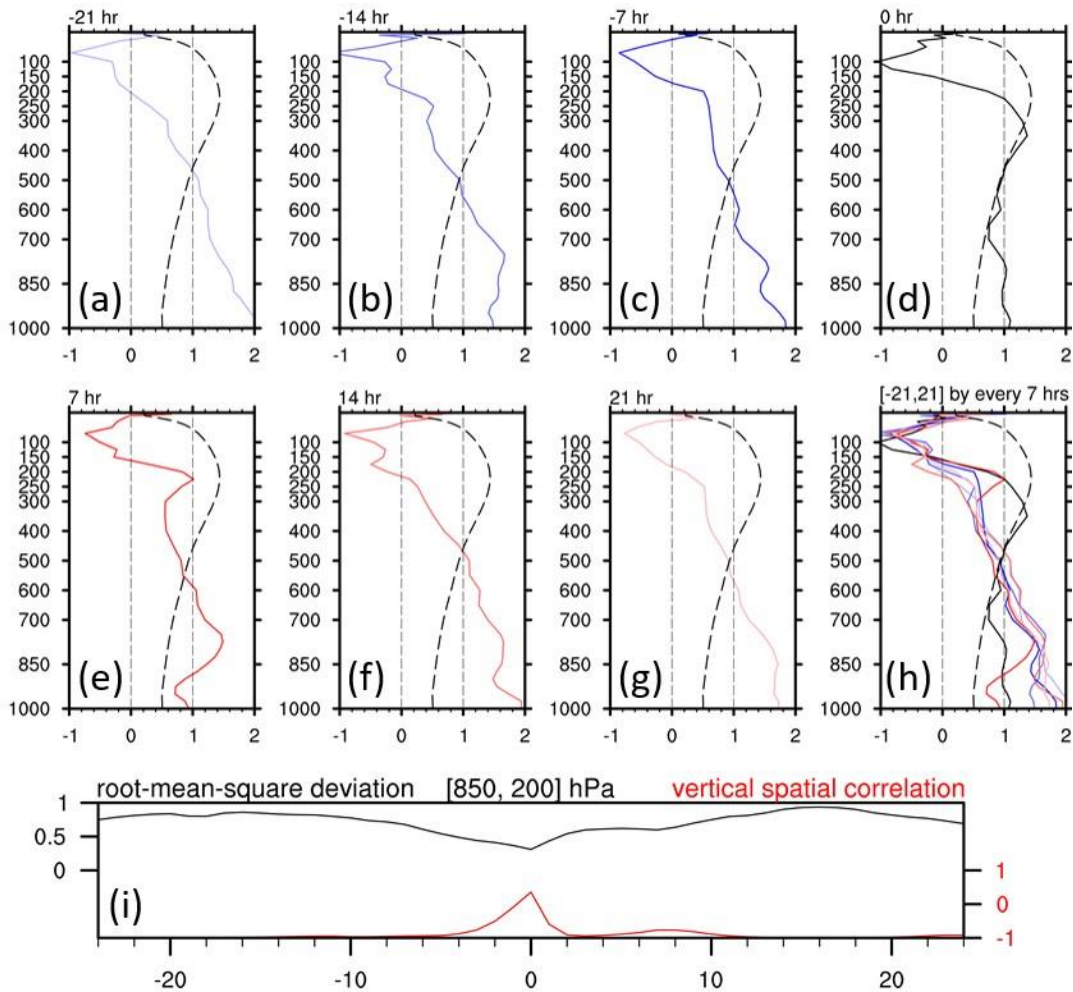
427 Takahashi, H., Luo, Z. J., & Stephens, G. L. (2017). Level of neutral buoyancy, deep convective outflow, and
428 convective core: New perspectives based on 5 years of CloudSat data. *Journal of Geophysical Research:*
429 *Atmospheres*, **122**(5), 2958-2969. <https://doi.org/10.1002/2016JD025969>

- 430 Takahashi, H., Luo, Z. J., & Stephens, G. (2021). Revisiting the Entrainment Relationship of Convective Plumes: A
431 Perspective From Global Observations. *Geophysical Research Letters*, **48**(6), e2020GL092349.
432 <https://doi.org/10.1029/2020GL092349>
- 433 Takahashi, H., Luo, Z. J., Stephens, G., & Mulholland, J. P. (2023). Revisiting the Land-Ocean Contrasts in Deep
434 Convective Cloud Intensity Using Global Satellite Observations. *Geophysical Research Letters*, **50**(5),
435 e2022GL102089. <https://doi.org/10.1029/2022GL102089>
- 436 Wang, D., Giangrande, S. E., Feng, Z., Hardin, J. C., & Prein, A. F. (2020). Updraft and Downdraft Core Size and
437 Intensity as Revealed by Radar Wind Profilers: MCS Observations and Idealized Model Comparisons.
438 *Journal of Geophysical Research: Atmospheres*, **125**(11), e2019JD031774.
439 <https://doi.org/10.1029/2019JD031774>
- 440 Wang, X., Zhang, G. J., & Suhas, E. (2022). Assessing free tropospheric quasi-equilibrium for different GCM
441 resolutions using a cloud-resolving model simulation of tropical convection. *Climate Dynamics*, **59**(9),
442 3035-3050. <https://doi.org/10.1007/s00382-022-06232-1>
- 443 Williams, A. I. L., Jeevanjee, N., & Bloch-Johnson, J. (2023). Circus Tents, Convective Thresholds, and the Non-
444 Linear Climate Response to Tropical SSTs. *Geophysical Research Letters*, **50**(6), e2022GL101499.
445 <https://doi.org/10.1029/2022GL101499>
- 446 Wu, T. (2012). A mass-flux cumulus parameterization scheme for large-scale models: description and test with
447 observations. *Climate Dynamics*, **38**(3), 725-744. <https://doi.org/10.1007/s00382-011-0995-3>
- 448 Wu, W., Dessler, A. E., & North, G. R. (2006). Analysis of the correlations between atmospheric boundary-layer
449 and free-tropospheric temperatures in the tropics. *Geophysical Research Letters*, **33**(20).
450 <https://doi.org/10.1029/2006GL026708>
- 451 Xu, K.-M., & Emanuel, K. A. (1989). Is the Tropical Atmosphere Conditionally Unstable? *Monthly Weather*
452 *Review*, **117**(7), 1471-1479. [https://doi.org/10.1175/1520-0493\(1989\)117<1471:ITTACU>2.0.CO;2](https://doi.org/10.1175/1520-0493(1989)117<1471:ITTACU>2.0.CO;2)
- 453 Yu, J.-Y., & Neelin, J. D. (1997). Analytic Approximations for Moist Convectively Adjusted Regions. *Journal of*
454 *the Atmospheric Sciences*, **54**(8), 1054-1063. [https://doi.org/10.1175/1520-0469\(1997\)054<1054:AAFMC>2.0.CO;2](https://doi.org/10.1175/1520-0469(1997)054<1054:AAFMC>2.0.CO;2)
- 455 Yuan, J., & Houze, R. A. (2010). Global Variability of Mesoscale Convective System Anvil Structure from A-Train
456 Satellite Data. *Journal of Climate*, **23**(21), 5864-5888. <https://doi.org/10.1175/2010JCLI3671.1>
- 457 Zeng, N., Neelin, J. D., & Chou, C. (2000). A Quasi-Equilibrium Tropical Circulation Model—Implementation and
458 Simulation. *Journal of the Atmospheric Sciences*, **57**(11), 1767-1796. [https://doi.org/10.1175/1520-0469\(2000\)057<1767:AQETCM>2.0.CO;2](https://doi.org/10.1175/1520-0469(2000)057<1767:AQETCM>2.0.CO;2)
- 459
460
- 461 Zhang, G. J., & McFarlane, N. A. (1995). Sensitivity of climate simulations to the parameterization of cumulus
462 convection in the Canadian climate centre general circulation model. *Atmosphere-Ocean*, **33**(3), 407-446.
463 <https://doi.org/10.1080/07055900.1995.9649539>
- 464 Zhang, Y., & Fueglistaler, S. (2020). How Tropical Convection Couples High Moist Static Energy Over Land and
465 Ocean. *Geophysical Research Letters*, **47**(2), e2019GL086387. <https://doi.org/10.1029/2019GL086387>
- 466 Zhao, M., Golaz, J.-C., Held, I. M., Guo, H., Balaji, V., Benson, R., et al. (2018). The GFDL Global Atmosphere
467 and Land Model AM4.0/LM4.0: 2. Model Description, Sensitivity Studies, and Tuning Strategies. *Journal*
468 *of Advances in Modeling Earth Systems*, **10**(3), 735-769. <https://doi.org/10.1002/2017MS001209>
- 469 Zheng, J., Liu, D., Wang, Z., & Wang, Y. (2018). Differences among three types of tropical deep convective clusters
470 observed from A-Train satellites. *Journal of Quantitative Spectroscopy and Radiative Transfer*, **217**, 253-
471 261. <https://doi.org/10.1016/j.jqsrt.2018.05.006>

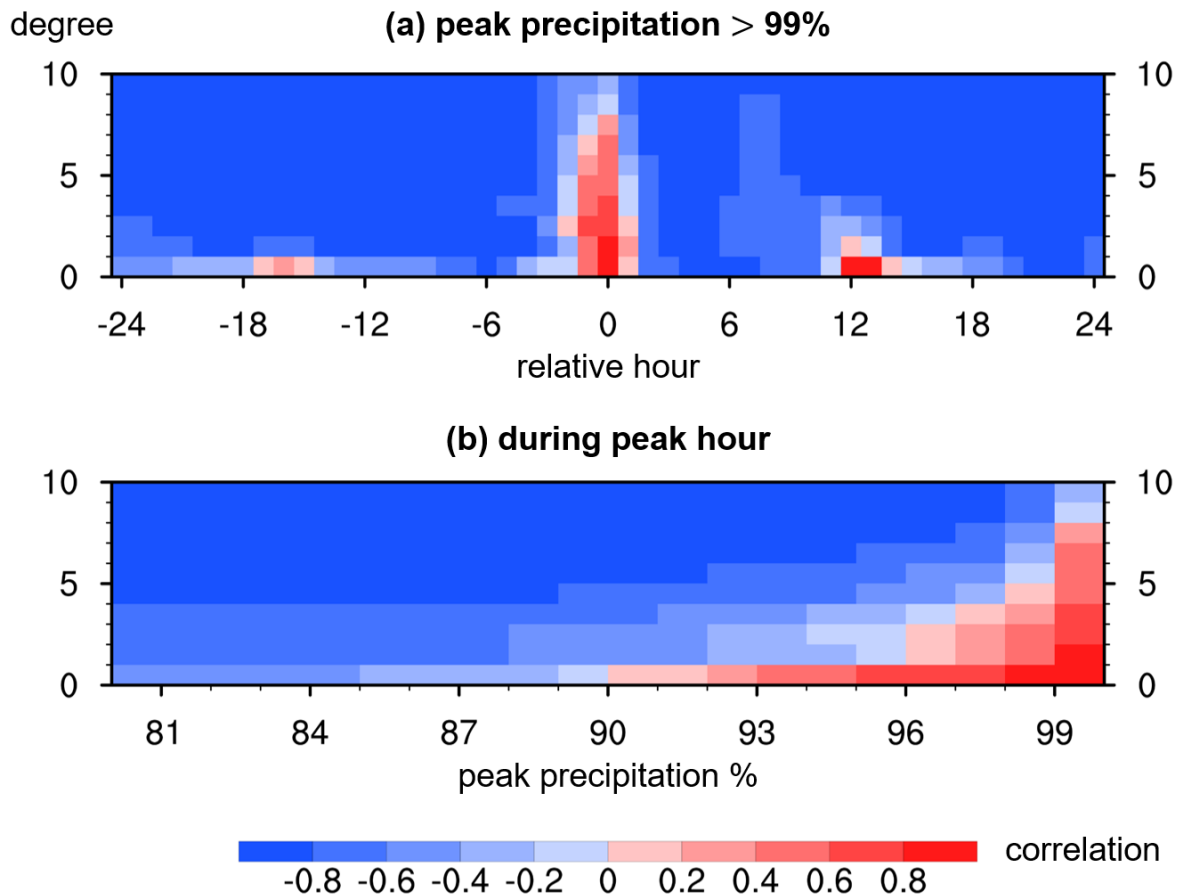


472 **Figure 1:** Occurrences of extracted temperature profiles within an 8-degree radius of tropical
 473 deep convection centers for (a) all instances regardless of peak precipitation and (b) instances
 474 where the peak precipitation surpasses the 99th percentile (c.f., method) in the year of 2013.

Within 8 deg, peak prec. > 8.337mm/hr (99%), 10555 profiles



475 **Figure 2:** (a) The A-profile (dashed) and vertical profile of regression coefficients (colored) of
 476 the temperature perturbations within an 8-degree radius conditioned on the peak precipitation
 477 exceeding the 99th percentile at each level against the free troposphere. The regression coefficient
 478 profile is calculated at -21 hour relative to the peak precipitation hour. (b-g) As in (a), but for -
 479 14, -7, 0, 7, 14, and 21 hours, respectively. Note that lighter colors indicate hours farther away
 480 from the 0 hour. (h) Collection of all the profiles shown in (a)-(g) for comparison. (i) The hourly
 481 time series of root-mean-square deviation (black) and vertical spatial correlation (red) between
 482 the A-profile and the regression coefficient profile over the troposphere.



483 **Figure 3:** (a) Vertical spatial correlation between the regression coefficient profiles using
 484 temperature perturbations conditioned on peak precipitation exceeding the 99th percentile and the
 485 A-profile over the free troposphere. Each box indicates the correlation at a specific hour relative
 486 to the peak precipitation (x-axis, spanning from -24 to 24 hour in 1-hour increments) within a
 487 certain radius with respect to the deep convection center (y-axis, extending from 1 to 10 degrees
 488 in 1-degree increments). (b) As in (a), but the correlations are calculated at the peak hour using
 489 temperature perturbations exceeding different percentile thresholds of the peak precipitation (x-
 490 axis, ranging from 80% to 99% in 1-percent increments).